

Dynamics of H atoms surface recombination in low-temperature plasma

V. Gubarev^{1,2,a}, D. Lopayev³, A. Zotovich³, M.A. Blauw⁴, V. Medvedev^{1,2}, P. Krainov^{1,2}, D. Astakhov², and S. Zyryanov^{3,5}

¹*Moscow Institute of Physics and Technology, Dolgoprudny, Russian Federation*

²*Institute of Spectroscopy of the Russian Academy of Science, Russian Federation*

³*Skobeltsyn Institute of Nuclear Physics, Moscow State University, Moscow, Russian Federation*

⁴*ASML, Veldhoven, Netherlands*

⁵*Faculty of Physics, Lomonosov Moscow State University, MSU, Moscow, Russia*

ABSTRACT

The dynamics of H atom recombination on materials of interest for a EUV lithographer was studied under a long-term low-pressure H₂ plasma exposure. The similarity of the experimental plasma with the typical EUV-induced plasma over the multi-layer mirrors (MLMs) surface of the EUV lithographic machine is demonstrated by means of 2D PIC MC simulation. The measurement of the temporal dynamics of the H atom surface loss probability (γ_H) is chosen for testing the surface modification during the treatment. Time-resolved actinometry of H atoms with Kr as the actinometer gas was used to detect the dynamics of the H-atom loss probability on the surface of Al, Ru, RVS and SiO₂. It is demonstrated that significant changes of the materials surface occur only at the very beginning of the treatment and are due to the surface heating and cleaning effects. After that no changes of the γ_H are found, indicating that the surface stays absolutely stable. A special test of the sensitivity of the used method to the state of surface was carried out. Dynamics of the γ_H changes with the small O₂ addition clearly demonstrated modification of the Al surface due to oxidation with the next removal of the oxygen by the H₂ plasma treatment. The rate of oxide removal is shown to be determined by plasma parameters such as the ion energy and flux to the surface.

I. INTRODUCTION

Extreme ultraviolet lithography (EUVL) is a crucial stage in the manufacturing of silicon microcircuits with a typical scale of the circuit features below 10 nm [1]. One of the key elements of the EUVL machine is a projection optical system [2,3]. The required lifetime of projection EUV optics should be rather long, up to ~ 30000 hours [4]. The EUV optics is a system of multilayer mirrors, MLMs. One of the main problems limiting the lifetime of EUV optics is contamination by carbon, tin etc. as well as surface oxidation [5,6]. In order to prevent contamination hydrogen gas atmosphere at $p \sim 5$ Pa is used which provides a cleaning process [1,7,8]. Molecular hydrogen buffer gas reduces tin penetration to the projection optics box. Besides, atomic hydrogen is able to create volatile compounds such as SnH_4 , CH_4 , H_2O that can be pumped out. The hot filament sources [9] of atomic hydrogen are commonly used for cleaning. However their application is challenging due to the big thermal loads on multi-layer mirrors and additional chemical pollution by filament material. Moreover, the rate of H cleaning is relatively low and requires large atom doses under the considered conditions.

Another approach for MLMs cleaning is to use EUV-induced plasma itself. During EUV pulse the high-energy photons ($h\nu = 92\text{eV}$) and secondary electrons, coming from the mirror surface ionize H_2 gas creating a plasma [10-12]. Ions and H atoms, coming from the plasma, interact with a lithographer walls and mirrors stimulating surface cleaning [13]. However, the plasma might also have a negative effect causing sputtering and blistering of MLMs as well as modification of EUV chamber materials [14]. Therefore, the knowledge on the behavior of such materials being under a long-time H_2 plasma exposure is of a special interest.

As known, the H atom surface loss probability is a sensitive function of the surface state and is able to reflect indirectly complex surface modifications. This work is devoted to the investigation of the dynamics of H atom surface loss probability on several materials of interest for EUV lithography, Al, Ru, RVS and SiO_2 , under a long-term exposure to low-pressure H_2 plasma under the conditions similar to the ones in the EUV-induced plasma.

II. 2D PIC SIMULATION

Plasma parameters in the EUV-induced plasma can vary in a wide range in dependence on the EUV pulse power density, pulse repetition rate, gas pressure etc. In order to simulate adequately the plasma conditions in the EUVL machine 2D PIC MC model has been developed [15]. As an example, the simulated energy spectrum of ion flux at an MLMs surface for typical EUV-plasma conditions (a normally incident beam with diameter fwhm = 2.4 cm onto a grounded surface, pulse duration 80 ns, pulse energy 1 mJ, H_2 pressure 5 Pa) is presented in fig.1. Red, green and blue points denote the ion energy distribution function (IEDF) of H^+ , H_2^+ , H_3^+ ions respectively; big black points depict the total calculated energy distribution of ion flux (IEDF) at the surface.

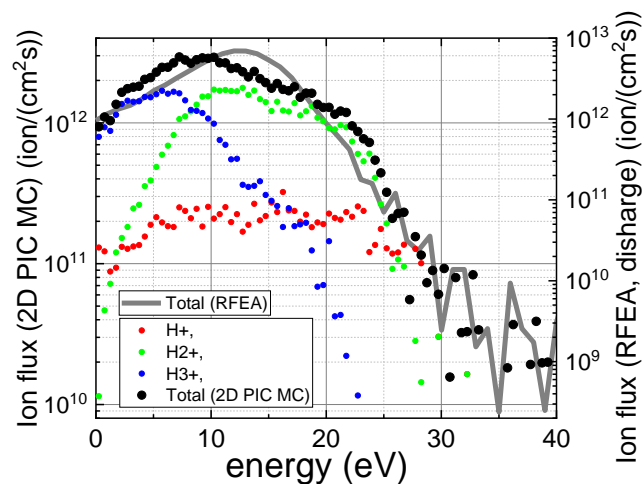


FIG. 1. The ion flux energy distribution (IEDF) (left vertical scale) from simulated EUV-induced plasma and SWD plasma (right vertical scale; see the text). Red blue, green and blue points denote IEDF of H^+ , H_2^+ , H_3^+ ions respectively, big black points depict the total calculated IEDF. The measured IEDF in SWD plasma is given by grey line. Simulation parameters: H_2 pressure is 5 Pa, EUV beam diameter is fwhm = 2.4 cm, EUV pulse energy is 1 mJ, EUV pulse duration is 80 ns. SWD parameters: H_2 pressure 40 Pa, input rf power 20W.

Two parts in the simulated spectrum might be distinguished: the first - closer to 0 eV and the second - above 20 eV. The first one corresponds to the IEDF in the EUV pulse afterglow when plasma is “cold” due to fast cooling of electrons. Such low-energy ions are able to assist the surface reactions with H atoms both coming from a gas phase as well as adsorbed on the surface. The second one corresponds to the IEDF during the EUV pulse when plasma is “hot” due to the continuous creation of a lot of energetic electrons. The total flux of these energetic ions even at a high repetition rate is lower than the flux of cold ions ($F_i < 10^{12}$ 1/($\text{cm}^2\cdot\text{s}$)). However, a large dose of such ions can produce accumulating effect affecting surface properties due to material sputtering and/or modification

owing to the hydrogen implantation into the surface layers. Such modification also influences the H atom surface recombination rate. In this work we focus on the evolution of H surface recombination rate at the different materials under a long-term exposure to “hot” H ions to estimate their effect on stability of EUV lithographer operation conditions.

III. EXPERIMENT

The similarity of the EUV-induced plasma parameters during the pulse with those in an electrode-less low-pressure plasma (like rf ICP and SWD) allows experimental reproducing of the “hot” part of IEDF of the EUV-plasma. In the current study a surface-wave discharge was used to study the dynamics of H atom recombination rate at various materials exposed to H₂ SWD plasma. The setup is schematically shown in fig.2. The SWD plasma was created in a quartz tube with a diameter 80 mm and length 50 cm while the metal flanges at the ends of the tube was closed by quartz plates (excepting small slits near the tube wall). The gas pressure varied in a range of 5 - 40 Pa by changing the gas flow rate in the range 5-20 sccm while the leak rate into the chamber was less than 0.005 sccm. Two copper ring electrodes located at distance of 2 cm from each other and driven at 81 MHz rf voltage (with rf power up to 50W) were used for creating the plasma inside the tube. The generator was connected to the electrodes through a matching network. The samples (thin rectangular plates) were placed inside the tube. The time-resolved actinometry of H atoms on Kr was used to measure H atom loss probability. The condenser collected emission from the quasi-neutral plasma volume above the sample and then the emission was focused on the entrance slit of the imaging spectrometer Solar TII MS 3504i (spectral resolution 0.3 nm FWHM) and detected by PMT (Hamamatsu R13456). The signal from PMT was transmitted to the NI DAQ board. The LabView program was used for the automation of the whole experiment: DAQ board measurements, flow meters, rf generator, modulator, database etc.

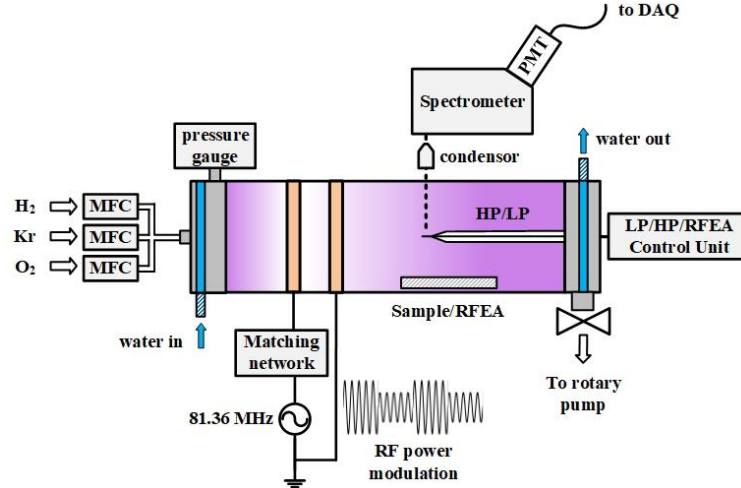


FIG. 2. Scheme of the experimental setup.

The energy spectrum and flux of ions falling on the sample surface were measured with Retarding Field Energy Analyzer (RFEA), Langmuir probe (LP) and MW hairpin probe. A flat rf-compensated RFEA placed at the sample position was used for measuring the ion energy distribution shape, while a Langmuir probe and MW hairpin probes were applied to measure electron temperature and plasma density respectively directly over the sample. The ion flux to the surface was evaluated from plasma density by using the classical formula for the flat collisionless sheath:

$$F_i \approx 0.5n_e V_B \quad (1)$$

where $V_B = \sqrt{\frac{T_e}{M_i}}$ - Bohm velocity, T_e - electron temperature, M_i - ion mass. We applied the formula (1) for the total pressure range (up to 40Pa) since the plasma sheath for grounded and floating samples is rather thin while the main ion in the considered conditions is H₃⁺ for which collisional and charge exchange cross sections with H₂ are small enough. In a considered range of input rf power, 5-100 W, and H₂ pressure, 5-40 Pa, the EEDF body is close to the Maxwellian one. It allowed estimating electron temperature which was varied in a range $T_e = 3.6-5.5$ eV. Thus, the main variation of ion flux to a sample is provided by varying the plasma density. The plasma density is almost a linear function of input power. The ion flux increases with input rf power and may be varied in the range of $F_i \sim 10^{13}-10^{16}$ (ion/(cm²s)). It should be noted that some discrepancy was observed in the n_e measured by hairpin and Langmuir probes. The n_e evaluated from Langmuir probe ion saturation current by using OML theory is always

higher while from the electron saturation current lower than the n_e measured by the hairpin probe [16]. The correction of the EEDF measured by Langmuir probe by extrapolating the measured EEDF by Maxwellian function to the plasma potential to compensate the electron drain and rf-incompensation effects gives plasma density comparable with the hairpin probe measurements [17] but increases an error. Thus the hairpin probe measurements were used for evaluating ion flux and dose at the sample surface.

The examples of the IEDF measured in SWD plasma for H_2 pressure 40 Pa with input rf power 20 W is presented by thick grey solid line in fig.1. It is seen that appropriate choice of discharge conditions allows simulating quite adequately the IEDF shape in EUV-induced plasma. At the same time, the SWD plasma demonstrates higher ion fluxes in comparison with EUV-induced plasma. Thus, SWD plasma conditions allows probing a very long EUV-induced plasma exposures (thousands of hours) of different materials during a reasonable period of time (hours).

Depending on the gas flow rate and input rf power it was possible to vary the IFED peak position from 5 eV up to the 55 eV. The higher pressure, the lower the IEDF peak energy. To treat the materials by high doses of "hot" ions the low-pressure regimes are more desirable due to a much shorter exposition time. Thus, the study was first of all focused on the regimes with gaspressure below 15 Pa.

Four different materials were exposed to H_2 SWD plasma. Those are plates of Al and RVS (stainless steel), thin 50 nm Ru films on quartz and SiO_2 (quartz chamber itself). The area of the SiO_2 sample was $1105cm^2$; RVS and Al - $50cm^2$; Ru - $25cm^2$. For Al, RVS and SiO_2 the maximum input power was 50 W, that provided the IEDF peak position at $\sim 50eV$ with ion flux $\sim 3 \cdot 10^{15}$ (ion/ cm^2s). In order to avoid overheating and blistering the Ru samples were exposed to weaker plasma at 10W that provided peak position of IED at $\sim 37eV$ with the total ion flux $\sim 1.5 \cdot 10^{15}$ (ion/ cm^2s).

IV. H ATOM LOSS RATE MEASUREMENTS: PULSED ACTINOMETRY METHOD.

For H atom loss rate measurements the approach proposed in [18,19] was applied. The sharp-edge small modulation of discharge power is used to get information about the slow recovery kinetics of H atom mole fraction under the given conditions, since plasma (both T_e and n_e) achieves its steady state during the modulation much faster than H atom density. It allows tracking changes of H density by using actinometry technique.

The concept of actinometry is transparent and well-known [19-21]. A small amount of actinometer (a few percent of a noble gas) is added to the gas flow in order not to disturb plasma parameters. Here 5% Kr was added to the H_2 flow. The emission lines of H and Kr are chosen the way that contribution of cascade relaxation and step-wise excitation processes to the corresponding atomic transitions is negligible in the considered conditions. The population and depopulation of the emitting atom states are mostly determined by i) direct excitation by electron impact, ii) dissociative excitation, iii) radiative decay and iv) collisional quenching. Thus, the ratio between the H and Kr atom densities can be written as follows:

$$\frac{n_H}{n_{Kr}} = \frac{I_{H^*}}{I_{Kr^*}} C_{Kr}^H - \frac{\alpha}{\xi} \quad (2)$$

where n_H and n_{Kr} are densities of H and Kr atoms in the ground state, $\xi = n_{Kr}/n_{H_2}$ - the mole fraction (percent) of krypton, $\alpha = k_{de}/k_e$ - the ratio of the H^* production rate constants by dissociative electron excitation and direct excitations from H_2 and H respectively. Under the considered conditions α is quite low that one can neglect the second term in eq.2. Actinometric coefficient C_{Kr}^H is defined by equation:

$$C_{Kr}^H = \frac{A_{nm} k_e^{Kr} (\sum A_{ij} + k_q^H n_{H_2})}{A_{ij} k_e^H (\sum A_{nm} + k_q^{Kr} n_{H_2})} \quad (3)$$

where A_{ij} and A_{nm} are Einstein's coefficients for hydrogen and krypton. k_q^H and k_q^{Kr} are rate constants of collisional quenching of the H and Kr emitting levels by molecular hydrogen. k_e^H and k_e^{Kr} are rate constants of electron impact excitation of H and Kr respectively. The excitation rate constants are determined by the excitation cross-sections, $\sigma_e(\varepsilon)$, of the corresponding levels and electron energy distribution function (EEDF), $f(\varepsilon)$:

$$k_e = \left(\frac{2e}{m_e} \right)^{1/2} \int_{E_{ex}}^{\infty} \sigma_e(\varepsilon) f(\varepsilon) \varepsilon d\varepsilon \quad (4)$$

where $\int f(\varepsilon)\sqrt{\varepsilon}d\varepsilon=1$, e and m_e are charge and mass of electron. Despite the excitation rate constants itself can noticeably vary depending on the plasma parameters, the ratio k_e^{Kr}/k_e^H remains almost constant with change of plasma parameters if an appropriate choice of H and Kr emitting states are made. If the difference in the excitation energies of the correspondin levels appears to be notably lower T_e , then ratio k_e^{Kr}/k_e^H remains almost constant. The following transitions of H atom with wavelength $\lambda = 656.6$ nm (excitation energy $E_{ex}\approx 12.09$ eV) and Kr atom with $\lambda = 811.3$ nm (excitation energy $E_{ex}\approx 12.06$ eV) were used. Thus, knowing the concentration of Kr and measuring the ratio of the chosen H and Kr lines intensities it is possible to evaluate H atoms concentration in the ground state.

Measurements of H atom loss frequency (and thereby H atom surface loss probability in the case when the surface loss is the dominant loss process) can be done by measuring dynamics of H atom concentration during the plasma modulation. To measure the rate of H atom surface recombination under the given conditions the time-resolved actinometry with $\sim 20\%$ plasma modulation has been applied. In the case of the plasma transition from one to another equilibrium states due to slight modulating rf power, the different plasma components reach their equilibrium values with characteristic times individual for each component. The characteristic relaxation times of the electron temperature and plasma density take units and tens of microseconds correspondingly. By contrast, the characteristic time of atomic hydrogen density recovery occurs at a millisecond time scale and determined by the surface loss. The modulation of T_e and n_e can lead to the noticeable modulation of H and Kr atoms emission, while the actinometric signal I_H/I_{Kr} allows ignoring the electron changes after T_e and n_e relaxation time and, therefore, tracking only the dynamics of H density. The dynamics of the actinometry signal was found measuring the dynamics of emission intensities of H and Kr atom lines with subtracting the dynamics of background emission near each line.

In the proposed method it is required to provide the so-called “kinetic regime” when H atom diffusion is fast enough and atom loss is determined by surface loss process. In this case, the H density should have a smoothed spatial profile in the chamber with small concentration gradients.

The hydrogen atom density profile measured by the actinometry method along the reactor tube at pressure $p = 15$ Pa is shown in fig.3a. The zero position corresponds to the center between the ring electrodes. The region from -3 cm to 3 cm (grey zone) corresponding to the plasma sheath areas (where plasma is not quasi-neutral) is excluded due to incorrect application of actinometric method in this area. H atom density was estimated using eq.2 in assumption of constant gas temperature ~ 450 K. As it is expected, H density profile has a small gradient from the electrodes to the ends of the tube due to the enhanced loss rate at the tube ends because of the metal presence (since H atom loss probability on metal is more than two orders higher in comparis with the one on SiO_2). The observed deviation from a constant H density profile is not critical and allows applying the actinometry method for kinetic measurements of H loss rate in the presence of samples in the reactor.

The top part of fig.3b shows an example of intensity dynamics of Kr (green curve) and H (red curve) emission lines and their ratio (blue curve) I_H/I_{Kr} is given in the bottom part. The results shown in fig. 3b correspond to the empty chamber (i.e. for fused silica). The exponential factors for growing and falling parts (red curve in the bottom graph of figure 3b) are almost the same and represent the characteristic loss time of the H atom at the chamber surface. The characteristic diffusion time of H atoms for the considered conditions (15 Pa and gas temperature ~ 450 K) is < 0.3 ms while the measured H loss time $\sim 3-4$ ms) [22], i.e. the diffusion of H atoms is much faster than the H atom surface loss. So, the loss frequency ν_H allows evaluating the hydrogen atom loss probability, γ_H :

$$\nu_H = \frac{S}{V} \frac{\gamma_H \nu_{th}^H}{2(2 - \gamma_H)} \quad (5)$$

where S/V is the so-called “geometric factor”, the ratio of the chamber area to the chamber volume); ν_{th}^H is the thermal velocity of hydrogen atoms; ν_H is the H loss frequency. The loss frequency for the empty chamber appeared to be rather stable allowing us to measure carefully loss rate changes when samples of Al, Ru or RVS were placed into the chamber. The loss rate at Al, Ru or RVS was then calculated from change in H loss frequency in comparison with the empty chamber with taking into account the area of the exposed materials. To minimize the possible Kr effect (above all, Kr^+ ions) on the material surface the Kr was admixed to hydrogen flow only during actinometric measurements. The actiniomeric measurements were fast enough (tens of seconds) that allowed us to study the evolution of the loss probability at different materials during the long-term (hours) plasma exposure.

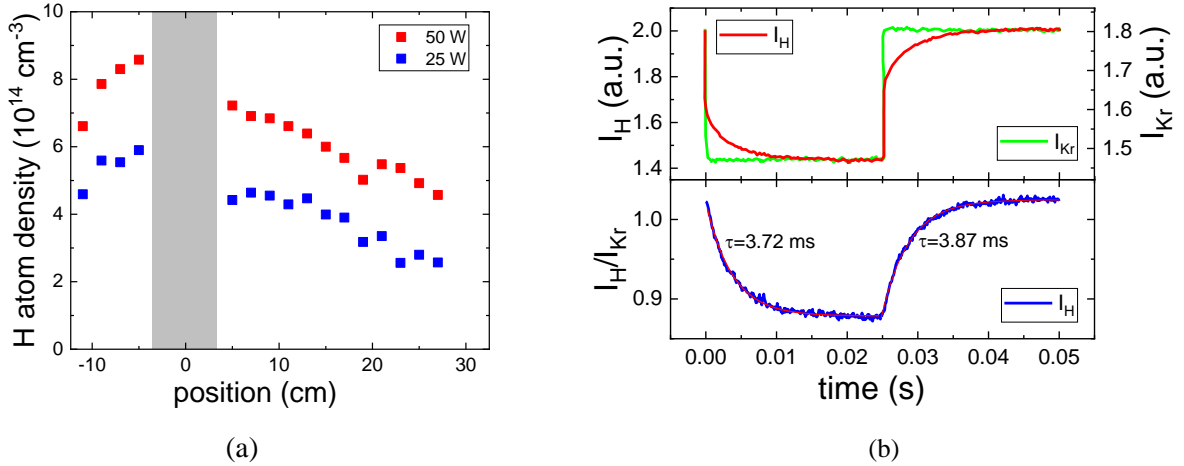


FIG. 3. a) Atomic hydrogen distribution along the experimental chamber at 15 Pa for SWD powers: 50W and 25W. Grey rectangle shows rf antenna area; b) Top graph - intensity evolution for Kr and H atoms. Bottom one - intensity ratio I_H/I_{Kr} . The exponential fitting of increasing/decreasing parts allows measuring the characteristic time of H-atoms surface loss and calculating the hydrogen surface loss probability according to eq.5.

V. RESULTS AND DISCUSSION

Fig.4a shows the measured evolution of the hydrogen atom surface loss probability (γ_H) on RVS (blue dots), Ru (green dots), Al (red dots) and SiO₂ (black dots) under a long time H₂ plasma exposure. The changes in γ_H during the first hours can be explained by the surface cleaning effect mainly from contaminations of carbon and oxidized layer. Besides, the samples heating may also promote the increase in H atom loss probability. After the “fluctuations” (during cleaning and heating) the H atom loss probability reaches the plateau for all the materials and remains constant with increasing exposure time. It shows that surface reaches the stable state and H₂ plasma doesn’t affect it. The values of H atom surface loss probability for the studied materials are presented in Table 1.

Table 1.

Material	H atom surface loss probability
SiO ₂	0.00314 ± 0.00006
Al	0.089 ± 0.004
Ru	0.127 ± 0.008
RVS	0.215 ± 0.005

Note here, that the trends for the surface state behavior are quite accurately reproduced by actinometric measurements of γ_H . However, the obtained absolute values of H atom surface loss probability might have an error up to ~30% because of atom density gradients over the samples and the used approach requires additional validation for obtaining absolute values, which is out of this work scope. Anyway, the obtained results for H atom loss probability on RVS and Al surfaces are in a good agreement with data obtained in the other works, for example in [22]. Thus, fig.4a shows that the long-term exposure to H₂ plasma, exactly H₃⁺ ions with energy below 50 eV, does not lead to a surface modification (except of the cleaning/heating processes) of the studied materials: RVS, Ru, Al and SiO₂ which are among the basic materials in EUV lithography tool.

It is also important to emphasize the very high sensitivity of the applied in this work methodology which allows detecting even small changes of surface state of materials. To demonstrate this and the mentioned above surface cleaning the experiment on a long time exposure of Al to plasma with addition of a small amount (5%) of O₂ to H₂ flow was carried out. As known, oxygen can strongly affect the surface state, first of all, due to oxidation process and hence change the hydrogen atom loss probability. The evolution of H atom loss probability on Al, when oxygen was and wasn’t added, is presented in the fig.4b. Vertical dashed lines display the moments of starting/stopping the oxygen flow.

The γ_H on Al evolution in fig.4b might be roughly splitted into 8 stages. The discharge power was 50W from 1st to 5th stages. At the 1st stage, the initial stable state of H atom loss probability is observed when oxygen flow is off. At the 2nd stage, the O₂ addition leads to the sharp decrease of H atom losses probability (it is seen like a rapid fall in fig.4b) apparently due to adsorption of oxygen atoms which block surface sites for H atom recombination (competitive recombination). At the 3rd stage, it replaced with a slower decrease in the H atom loss probability most probably due to Al surface oxidation. The 4th stage corresponds to the moment when oxygen flow was turned off. Now verse visa, a sharp rise of H atom loss probability occurs, apparently due to removal of adsorbed oxygen atoms and, therefore, unblocking sites for H atom recombination. However at the 5th stage the γ_H reduction observed at the

3^d stage partly continued further probably owing to continuing reconstruction of Al-O surface layer. It goes with gradual slowing down and almost stopping of the γ_H change to the 6th stage. At the 6th stage the H₂ discharge power was increased to 75W after that the γ_H started to increase due to H₂ plasma cleaning of oxidized Al layer (removal of oxygen from the surface layers). At the 7th stage, the higher rate of the γ_H increase is observed after the input rf power was further increased to 100W. Finally, at the 8th stage, when oxygen is fully removed and Al surface is almost recovered, H atom loss probability is stabilized at the level slightly higher than in the beginning at the 1st stage due to the higher temperature of Al sample (because of the higher input rf power - 100W against the 50W in the beginning). Thus the applied method clearly demonstrates high sensitivity to the surface state, for example, to the process of oxygen removal from the oxidized layers by H₂ plasma.

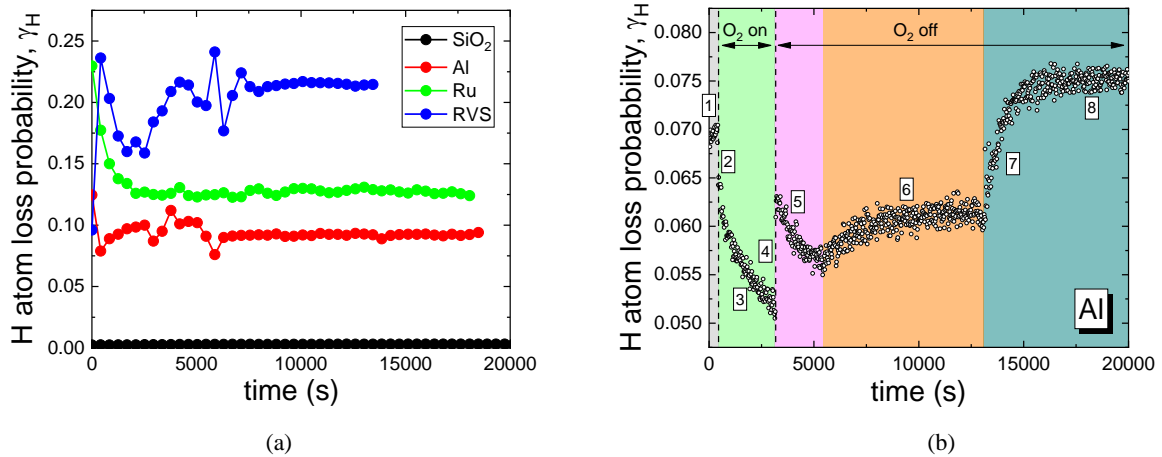


FIG. 4. a) Evolution of the H atom surface loss probability on RVS (green), Ru (violet), Al (red), SiO₂ (blue curve) samples under H₂ plasma exposure. The area of the SiO₂ sample was 1105cm²; RVS and Al - 50cm²; Ru - 25cm². b) Evolution of the H atom loss probability on Al surface with addition of 5% O₂ (in the time interval $t = 280\text{s} - 2900\text{s}$) and variation of the discharge power. Details of the evolution stages are presented in the text. The discharge power is for 1st-5th stages – 50W, for 6th – 75W and for 7th and 8th – 100W.

VI. CONCLUSION

In this work, the evolution of the H atom loss probability, γ_H , on the different materials (RVS, Al, Ru, SiO₂) being of interest in EUV lithography was investigated under the long time exposure to low-pressure SWD hydrogen plasma. 2D PIC model was applied to demonstrate that SWD plasma under the applied discharge conditions can adequately simulate the ion flux energy distribution on a mirror surface in EUV-induced plasma. The measurements of γ_H clearly show the plasma cleaning effect on all the studied materials during the first two hours. After that the H atom loss probability remains constant under the long time plasma exposure (with ion energy $\sim 50\text{eV}$ and flux $\sim 10^{15}$ ions/(cm²s) at the sample surface). It shows that after cleaning, H₂ plasma doesn't modify the surface of the cleaned materials.

By admixture of a small amount of O₂ to H₂ it was shown that oxidation decreases the H atom recombination rate. It was also shown that H₂ plasma is able to remove oxygen from the oxidized layers and the removal rate is growing with rf power mostly due to increasing of ion energy and flux.

ACKNOWLEDGMENTS

S. Zyryanov would like to acknowledge Russian Science Foundation: RSF research project No.2172-10040. D. Lopaev, A. Zotovich and S. Zyryanov are also grateful to the Interdisciplinary Scientific and Educational School of Moscow University 'Photonic and Quantum Technologies. Digital Medicine.' for support.

REFERENCES

- [1] N. Fu, Y. Liu, X. Ma, and Z. Chen. *J. Microelectron. Manuf.* **2** (2019) 19020202
- [2] A. Erdmann. "Optical and EUV lithography: A modeling perspective," **PM323** (2021) ISBN:9781510639010
- [3] M. Sascha, C. Zeiss, K. Winfried, J. Timo, E. Hartmut, and H. Dirk. "EUV lithography, second edition," **PM283** (2018) ISBN:9781510616783
- [4] B. Mertens, M. Weiss, H. Meiling, R. Klein, E. Louis, R. Kurt, M. Wedowski, H. Trenkler, B. Wolschrijn, R. Jansen, A. Runstraat, R. Moors, K. Spee, S. Ploger, and R. Kruijs. *Microelectronic Engineering* **74** (2004) 16-22
- [5] J.T. Hollenshead, L.E. Klebanof and G. Delgado. *Journal of Vacuum Science and Technology B* **37** (2019) 021602
- [6] J. Chen. Characterization of EUV induced contamination on multilayer optics, Ph.D. thesis: University of Twente (2011).
- [7] N. Bowering and C. Meier. *Journal of Vacuum Science and Technology B* **36** (2018) 021602

- [8] V. Bakshi, "EUV Lithography". Second Edition: Bellingham. Society of Photo-Optical Instrumentation Engineers (SPIE) (2018)
- [9] M. Kerkhof, M. Waiblinger, J. Weber, C. Baur, A. Nikipelov, and C. Cloin. SPIE 11609, Extreme Ultraviolet (EUV) Lithography XII, 116090N (2021)
- [10] J. Beckers, T. Ven, R. Horst, D. Astakhov, and V. Banine. *Applied Sciences* **9** (2019) 2827
- [11] T. Ven, P. Reefman, C. Meijere, R. Horst, M. Kampen, V. Banine, and J. Beckers. *Journal of Applied Physics* **123** (2018) 063301
- [12] M. Kerkhof, A.M. Yakunin, D. Astakhov, M. Kampen, R. Horst and Vadim Banine. *J. Micro/Nanopattern. Mater. Metrol.* **20** (2021) 033801
- [13] A. Dolgov, D. Lopaev, T. Rachimova, A. Kovalev, A. Vasilyeva, C. Lee, V. Krivtsov, O. Yakushev, and F. Bijkerk. *Journal of Physics D: Applied Physics* **47** (2014) 025102
- [14] C. Onwudinanti, G. Brocks, V. Koelman, T. Morgana, and S. Tao. *Phys. Chem. Chem. Phys.* **23** (2021) 13878
- [15] D. Astakhov, Numerical study of extreme-ultra-violet generated plasmas in hydrogen, Ph.D. thesis: University of Twente (2016).
- [16] V. Godyak and V. Demidov. *Journal of Physics D: Applied Physics* **44** (2011) 233001
- [17] D. Lopaev, M. Bogdanova, A. Volynets, A. Zotovich, and S. Zyryanov. *Plasma Sources Science and Technology* **29** (2020) 025026
- [18] D.V. Lopaev, A.V. Smirnov. *Plasma Physics Reports* **30** (2004) 882
- [19] J.P. Booth, O. Guaitella, A. Chatterjee, C. Drag, V. Guerra, D. Lopaev, S. Zyryanov, T. Rakhimova, D. Voloshin and Yu. Mankelevich. *Plasma Sources Sci. Technol.* **28** (2019) 055005
- [20] A. Gottscho and M. Donnelly, *Journal of Applied Physics* **56** (1984) 245
- [21] D. Lopaev, A. Volynets, S. Zyryanov, A. Zotovich, and A. Rakhimov. *Journal of Physics D: Applied Physics* **50** (2017) 075202
- [22] M. Sode, T. Schwarz-Selingerand, W. Jacob, and H. Kersten. *Journal of Applied Physics* **116** (2014) 013302